Collapse of the hyperfine magnetic field at the Ru site in ferromagnetic rare earth intermetallics

D. Coffey

Dept. of Physics, Buffalo State College, Buffalo, New York 14222

M. DeMarco

Dept. of Physics, Buffalo State College, Buffalo,

New York 14222 and Dept. of Physics, SUNY Buffalo, Buffalo, NY 14260

P. C. Ho

Dept. of Physics, California State, Fresno CA 93740

M. B. Maple and T. Sayles

Dept. of Physics, University of California, San Diego CA 92093

J. W. Lynn and Q. Huang

NIST Center for Neutron Research,

National Institute of Standards and Technology, Gaithersburg, MD 20899

S. Toorongian and M. Haka

Nuclear Medicine Department, State University of New York, NY 14260.

(Dated: October 15, 2009)

Abstract

The Mössbauer Effect(ME) is frequently used to investigate magnetically ordered systems. One usually assumes that the magnetic order induces a hyperfine magnetic field, $B_{hyperfine}$, at the ME active site. This is the case in the ruthenates, where the temperature dependence of $B_{hyperfine}$ at ^{99}Ru sites tracks the temperature dependence of the ferromagnetic or antiferromagnetic order. However this does not happen in the rare-earth intermetallics, $GdRu_2$ and $HoRu_2$. Specific heat, magnetization, magnetic susceptibility, Mössbauer effect, and neutron diffraction have been used to study the nature of the magnetic order in these materials. Both materials are found to order ferromagnetically at 82.3 and 15.3 K, respectively. Despite the ferromagnetic order of the rare earth moments in both systems, there is no evidence of a correspondingly large $B_{hyperfine}$ in the Mössbauer spectrum at the Ru site. Instead the measured spectra consist of a narrow peak at all temperatures which points to the absence of magnetic order. To understand the surprising absence of a transferred hyperfine magnetic field, we carried out *ab initio* calculations which show that spin polarization is present only on the rare-earth site. The electron spin at the Ru sites is effectively unpolarized and, as a result, $B_{hyperfine}$ is very small at those sites. This occurs because the $4d$ Ru electrons form broad conduction bands rather than localized moments. These $4d$ conduction bands are polarized in the region of the Fermi energy and mediate the interaction between the localized rare earth moments.

PACS numbers: 76.80.+y, 71.20.Lp, 28.20.Cz, 75.50.Cc, 75.60.Ej, 75.40.-s

I. INTRODUCTION

Compton and Matthias[1] found that superconductivity and ferromagnetism occur in Laves phase compounds containing lanthanide elements and Ru. This led to the suggestion that superconductivity and ferromagnetism could coexist in $Ce_{1-x}R_xRu_2$ alloys, since superconductivity occurs below 6 K in $CeRu_2$ and ferromagnetism is present in that temperature range in RRu_2, where R is Gd or Ho[2]. The phase diagram for $Ce_{1-x}R_xRu_2$ was investigated by Wilhelm and Hillebrand[3] for R=Gd, Ho, Dy, Pr. Although no long range magnetic order was found in the superconducting region of the phase diagrams of these alloys, evidence for short-range order was found in the temperature dependence of the ^{155}Gd ME and in nuclear quadrupole resonance measurements. This occurs in $Ce_{1-x}Gd_xRu_2$[4, 5] for a narrow range of doping about $x \sim 0.1$. Fischer and Peter[6] pointed out that the specific heat of $Ce_{1-x}Gd_xRu_2$ measured by Peter et al.[7] also showed an anomalous temperature dependence. The specific heat divided by temperature, $\frac{C}{T}$, for $CeRu_2$ showed a sharp jump at the superconducting transition and a rapid fall off to zero as $T \rightarrow 0$, as expected. However the jump becomes more rounded in $Ce_{1-x}Gd_xRu_2$ as x increases and $\frac{C}{T}$ increases as $T \rightarrow 0$. The value of $\frac{C}{T}$ as $T \rightarrow 0$ increases as x increases from 0.05 to 0.11. This anomalous temperature dependence was taken as evidence of a ferromagnetic contribution to $\frac{C}{T}$. The analysis of the data did not provide a microscopic model for the nature of this contribution or explain how it could coexist with superconductivity.

Evidence for the coexistence of superconductivity and short-range ferromagnetic correlations was also found in $Ce_{0.73}Ho_{0.27}Ru_2$ from the temperature dependence of the ^{57}Fe ME below $\sim$2 K and from neutron scattering data[8, 9, 10]. Since the hyperfine coupling constant of Ru is twice that of Fe[11] it was expected that there would be a magnetic field at the Ru nucleus of about 15 T in this material. Hyperfine magnetic fields were reported at the Gd site in $Ce_xGd_{1-x}Ru_2$[4] for $x > 0.2$, whose temperature dependence was consistent with the Curie temperature. More recently, Andoh discussed the magnetic properties of a number of the RRu_2[12].

$CeRu_2$ has been assigned to have the cubic Laves structure($Fd\bar{3}m$), although recently Huxley et al.[13] have shown that its symmetry is lowered due to a slight variation in the displacement of the Ru from their cubic Laves positions. $GdRu_2$ and $HoRu_2$ are in the

hexagonal Laves phase structure ($P6_3/mmc$). $GdRu_2$ has also been reported in the cubic Laves phase.[14] The difference in structure does not determine whether the ground state is superconducting or ferromagnetic since $NdRu_2$, a ferromagnet, has the $Fd\bar{3}m$ structure. Here we concentrate on reconciling the ferromagnetism found in neutron scattering, transport, and thermodynamic measurements with Mössbauer spectroscopy.

Mössbauer spectroscopy is a nuclear probe of the electronic properties of systems which has been used to investigate magnetic order in many systems. The evidence of magnetic order appears in the Mössbauer spectrum as a hyperfine magnetic field induced at the nucleus at which the Mössbauer Effect(ME) is measured. In this way the temperature dependence of magnetic order has been probed by the ^{99}Ru ME in both ferromagnetic and antiferromagnetic ruthenates[15, 16]. The magnetic order has also been investigated using the ^{57}Fe, ^{193}Ir, and ^{155}Gd ME in the intermetallic compounds of interest here. One can distinguish between two cases. In the first case the $B_{hyperfine}$ is found at a site on which there is an ordered electronic moment. This is the case of the ruthenates and a number of rare earth intermetallics. Using the ^{57}Fe ME, Wertheim and Wernick[17] measured $B_{hyperfine}$ values in RFe_2(R=Ce, Sm, Gd, Dy, Ho, Er, Tm). $B_{hyperfine}$ is found to be $\sim$23T in spite of the wide range in the size of the localized moments on the R sites. By comparison, the value for $B_{hyperfine}$ in ferromagnetic Fe is 32 T. The ^{57}Fe ME has also been used to investigate the magnetic structure in rare earth iron ternary intermetallics.[18] De Graaf et al.[19] extracted a value for $B_{hyperfine}$ equal to 17.5T at the Gd site in $GdCu_2$ using ^{155}Gd ME from a structureless spectrum.

In the second case, for a non-magnetic ion in a magnetically ordered lattice, the measured ME at this site is expected to show evidence of the magnetic order through a transferred hyperfine magnetic field. Transferred hyperfine fields at the non-magnetic Ir site were measured by Atzmony et al.[20] in RIr_2(R=Pr,Nd,Sm,Gd,Tb,Dy,Ho). They found a wide variation from 4 T in $HoIr_2$ to 19 T in $GdIr_2$. Transferred hyperfine fields have also been measured in a rare-earth matrix doped with 1% Sn and in R_2Sn using the ^{119}Sn ME[21]. For Sn doped into a rare earth, these range from -5.3 T in a Tm matrix to 23.8 T in a Gd matrix. The values of $B_{hyperfine}$ are linear in the projection of the spin of the rare earth moment on its total angular momentum, $(g-1)J$. In R_2Sn, these fields range from -5.5 T (Er_2Sn) to 28.9 T (Gd_2Sn).

The fact that the sign of the transferred hyperfine field can change suggested that there is competition between different contributions which align or antialign the nuclear moment with the ordered electronic moment. A negative hyperfine magnetic field is antiparallel to the ordered electronic moment. Watson and Freeman were among the first to investigate the origin of the hyperfine magnetic field with large scale numerical calculations based on the Hartree-Fock approximation[22, 23]. Although these calculations were limited by the computational capabilities then available, they demonstrated a number of the qualitative features of the experimental data. In particular, they showed that the ordered $4f$ moment in Gd polarizes the electron density in the opposite direction to the ordered $4f$ moment very close to the nucleus and in the region beyond localized $4f$ bands at the edge of the Gd ion. They showed that the largest contribution to the hyperfine magnetic field due to polarization of the spin density of s electrons is the result of contributions of different signs from different s-shells. Their calculations also showed that the polarization of the spin density on neighboring sites could be opposite to that of the ordered moments leading to the negative hyperfine magnetic field. The sign of the transferred hyperfine field can be modulated by varying the lattice constant, as we describe in the section on calculations of the electronic properties below. In the calculations of Watson and coworkers, it was assumed that the $5s$ electrons formed the conduction band which turns out not to be the case in $GdRu_2$, as we will also discuss below. In addition orbital contributions to transferred hyperfine magnetic field, based on the assumption that it arises from the coupling of f electrons on the rare earth sites with s-conduction electrons, were investigated by Dunlap et al.[24] Local Spin Density Approximation(LSDA) calculations were first used to calculate hyperfine magnetic fields in ferromagnetic $3d$ metals by Callaway and Wang[25, 26]. We use a more recent implementation of the LSDA to calculate hyperfine fields on Ru sites and compare with our measured values.

We present magnetic, transport and thermodynamic data on $GdRu_2$, and magnetic and neutron diffraction data on $HoRu_2$, showing that these are ferromagnetically ordered at low temperatures. However, our ME measurements of $GdRu_2$ and $HoRu_2$ show that $B_{hyperfine}$ at the Ru site is so small that, without the evidence of other experiments, one would conclude that there is no magnetic order. The almost complete collapse of the value of $B_{hyperfine}$ is an unexpected result in materials whose Curie temperatures are 82.3 K and 15.3 K,

respectively. Interestingly, the absence of $B_{hyperfine}$ at the Ru sites in $GdRu_2$ was noted previously without comment[27].

We calculate the electronic properties of these materials using a spin polarized fully relativistic all-electron linearized augmented plane wave method[28]. *ab initio* bandstructure calculations have previously been used by other authors to determine hyperfine magnetic fields and electric field gradients (EFG).[29, 30, 31, 32] We find good agreement between the EFG tensor and that found from the Mössbauer spectra of $CeRu_2$. We also find that the calculated $B_{hyperfine}$ at the Ru sites in $GdRu_2$ and $HoRu_2$ are much smaller than those on Gd and Ho, consistent with the experimental results. First we present the experimental results.

II. EXPERIMENTAL RESULTS

A. Evidence of Ferromagnetism

The transport and thermodynamic properties of $GdRu_2$ were investigated with a number of probes. The temperature, T, dependence of electrical resistance, R, and the slope $\mathrm{d}R/\mathrm{d}T$ of a polycrystalline sample of $GdRu_2$ are plotted in Fig. 1. A breaking curvature in R, accompanied by a sharp increase of $\mathrm{d}R/\mathrm{d}T$, occurs at $\sim 86\,\mathrm{K}$ as temperature decreases, which is due to the development of an ordered state. The dc-magnetic susceptibility χ_{dc} is measured from 1.9 K to 300 K at an applied magnetic field $H = 50\,\mathrm{Oe}$ in the zero field cooled (ZFC) and field cooled (FC) states and the data are displayed in Fig. 2. Hysteresis in $\chi_{\mathrm{dc}}(T)$ appears at $\sim 83\,\mathrm{K}$. A Curie-Weiss analysis was done on the molar magnetic susceptibility data χ_{mol} given by

$$\chi_{\mathrm{mol}} = \frac{1}{3}\frac{N_{\mathrm{A}}\mu_{\mathrm{eff}}^2}{k_{\mathrm{B}}(T-\Theta_{\mathrm{CW}})}, \tag{1}$$

where N_{A} is the Avogadro's number, $\mu_{\mathrm{eff}} = g(JLS)\sqrt{J(J+1)}\mu_B$ is the effective magnetic moment, $g(JLS)$ is the Landé g-factor, k_{B} is the Boltzmann's constant, and Θ_{CW} is the Curie-Weiss temperature. A positive $\Theta_{\mathrm{CW}} \sim 85\,\mathrm{K}$ indicates a ferromagnetic order in $GdRu_2$ and $\mu_{\mathrm{eff}} \approx 7.6\,\mu_B$ (Bohr magneton), which is close to the theoretical value $7.94\,\mu_B$ of the free ion moment of Gd^{3+}. This value of Θ_{CW} is consistent with the temperature at which hysteresis first appears.

Arrott plots of magnetization M with respect to the internal magnetic flux density $\mu_0 H_{\mathrm{int}}$

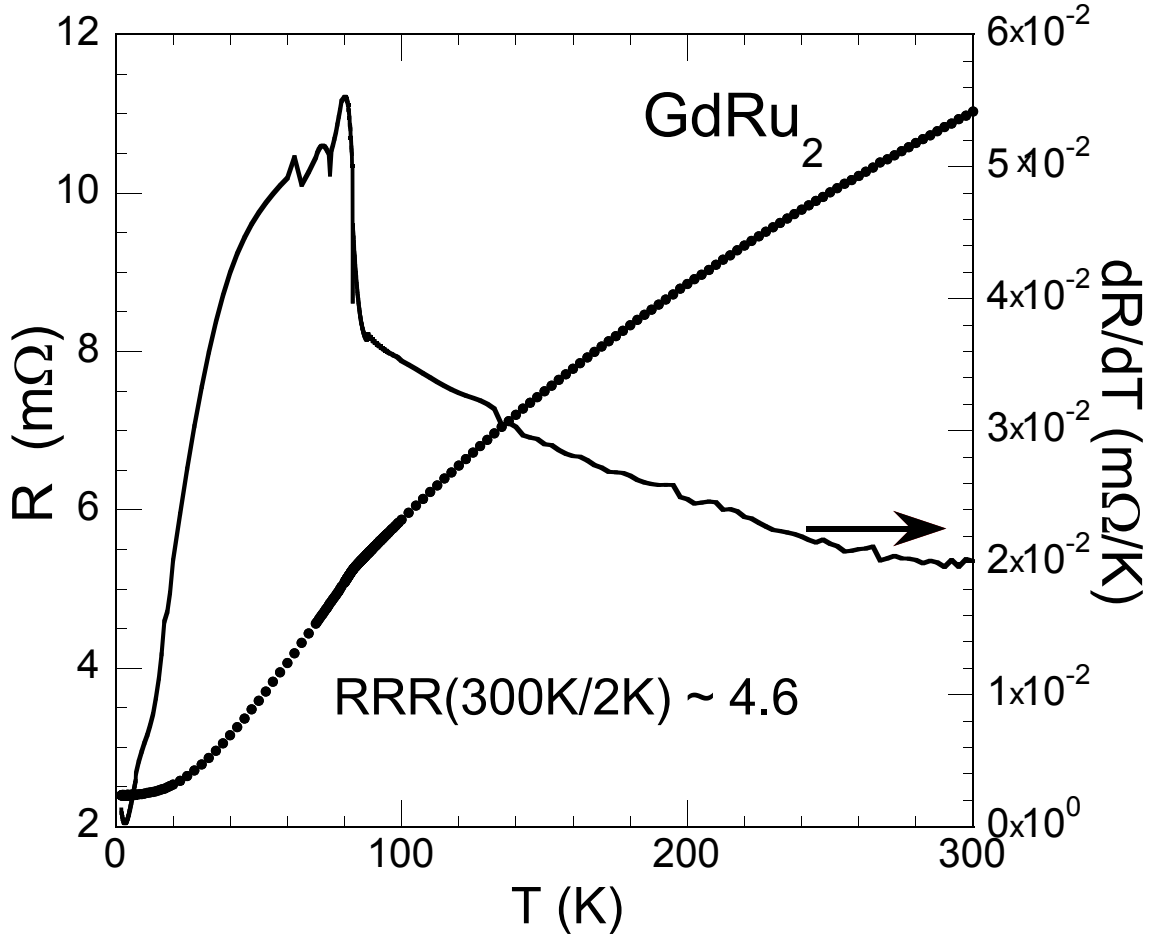

FIG. 1: Temperature T dependence of resistance R and the slope dR/dT of a polycrystalline sample of $GdRu_2$. The value of the residual resistivity ratio RRR(300 K/2 K) is ~ 4.6. A curvature breaking which occurs in the $R(T)$ data at ~ 80 K corresponds to the transition temperature of magnetic order.

divided by M were constructed in an attempt to determine the Curie temperature T_C more accurately. A conventional Arrott plot consisting of M^2 vs $(\mu_0 H_{\rm int}/M)$ isotherms, is shown in Fig. 3(a). In the simplest mean-field analysis of ferromagnetism, M^2 vs $(\mu_0 H_{\rm int}/M)$ isotherms form a series of parallel straight lines near T_C, and the isotherm passing through the origin corresponds to T_C. However, the M^2-$(\mu_0 H_{\rm int}/M)$ isotherms of $GdRu_2$ are slightly curved. Therefore, we applied a modified Arrott plot $M^{1/\beta}$ vs $(\mu_0 H_{int}/M)^{1/\gamma}$, where $\beta \sim 0.28$ and $\gamma \sim 0.98$ are the critical exponents based on the Arrott-Noakes equation [33], and the results are plotted in Fig. 3(b). The value of T_C is ~ 82.3 K.

Figure 4(a) shows the specific heat C of $GdRu_2$ from 2 K to 300 K. As T decreases to

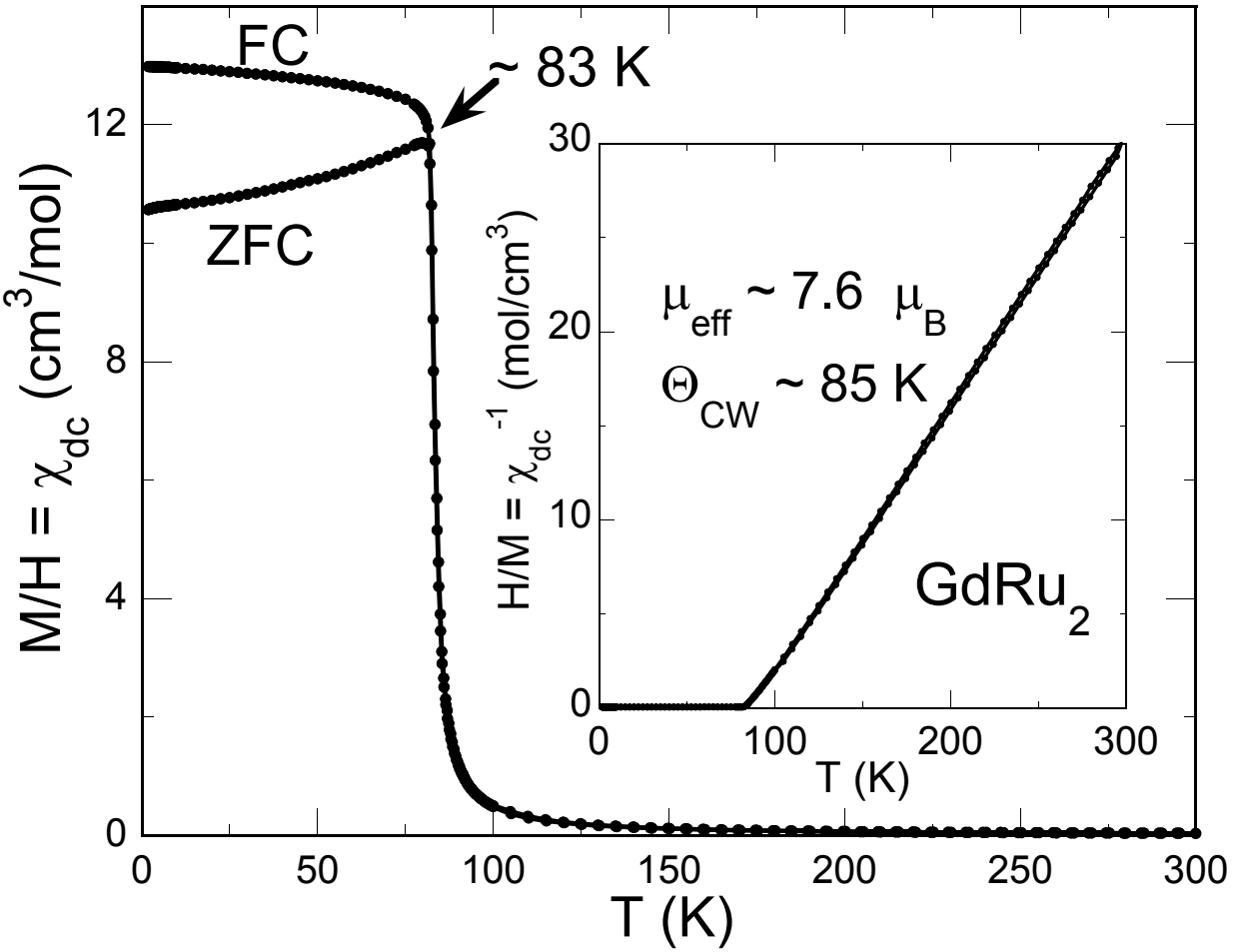

FIG. 2: Temperature dependence of dc-magnetic susceptibility $\chi_{\rm dc}$ of $GdRu_2$ measured at an applied magnetic field $H = 50\,\mathrm{Oe}$. Hysteresis occurs at $T \sim 83\,\mathrm{K}$, coinciding with the Curie temperature $\mathrm{T_C}$ determined from the modified Arrott plot[33]. $\chi_{\rm dc}^{-1}$ vs T is shown in the inset and follows a Curie-Weiss behavior, which results in an effective moment $\mu_{\rm eff} \sim 7.6\mu_{\rm B}$ and a Curie-Weiss temperature $\Theta_{\rm CW} \sim 85\,\mathrm{K}$.

$\sim 87\,\mathrm{K}$, C starts to rise and peaks at $\sim 81\,\mathrm{K}$, indicating the ferromagnetic second order phase transition. From the C/T vs T^2 analysis between 7 K and 14 K (inset of Figure 4(b)), the values of the electronic specific coefficient γ and the Debye temperature $\Theta_{\rm D}$ of $GdRu_2$ are estimated to be 29 mJ/mol-K, and 200 K, which seem reasonable in comparison with $LaRu_2$'s $\gamma \sim 41.6\,\mathrm{mJ/mol\text{-}K}$ and $\Theta_{\rm D} \sim 158.4\,\mathrm{K}$. [34] After subtraction of electron and phonon contributions $C_{\rm e}(T) + C_{\ell}(T)$ from C(T) (Fig. 4(a)), the temperature dependence of the estimated magnetic entropy $S_{\rm mag}$ is displayed in Fig 4(b). Estimated $S_{\rm mag}$ reaches a saturated value of 1.5 R above $\mathrm{T_C}$ which is lower than the expected value of Rln8 ($\approx$ 2R).

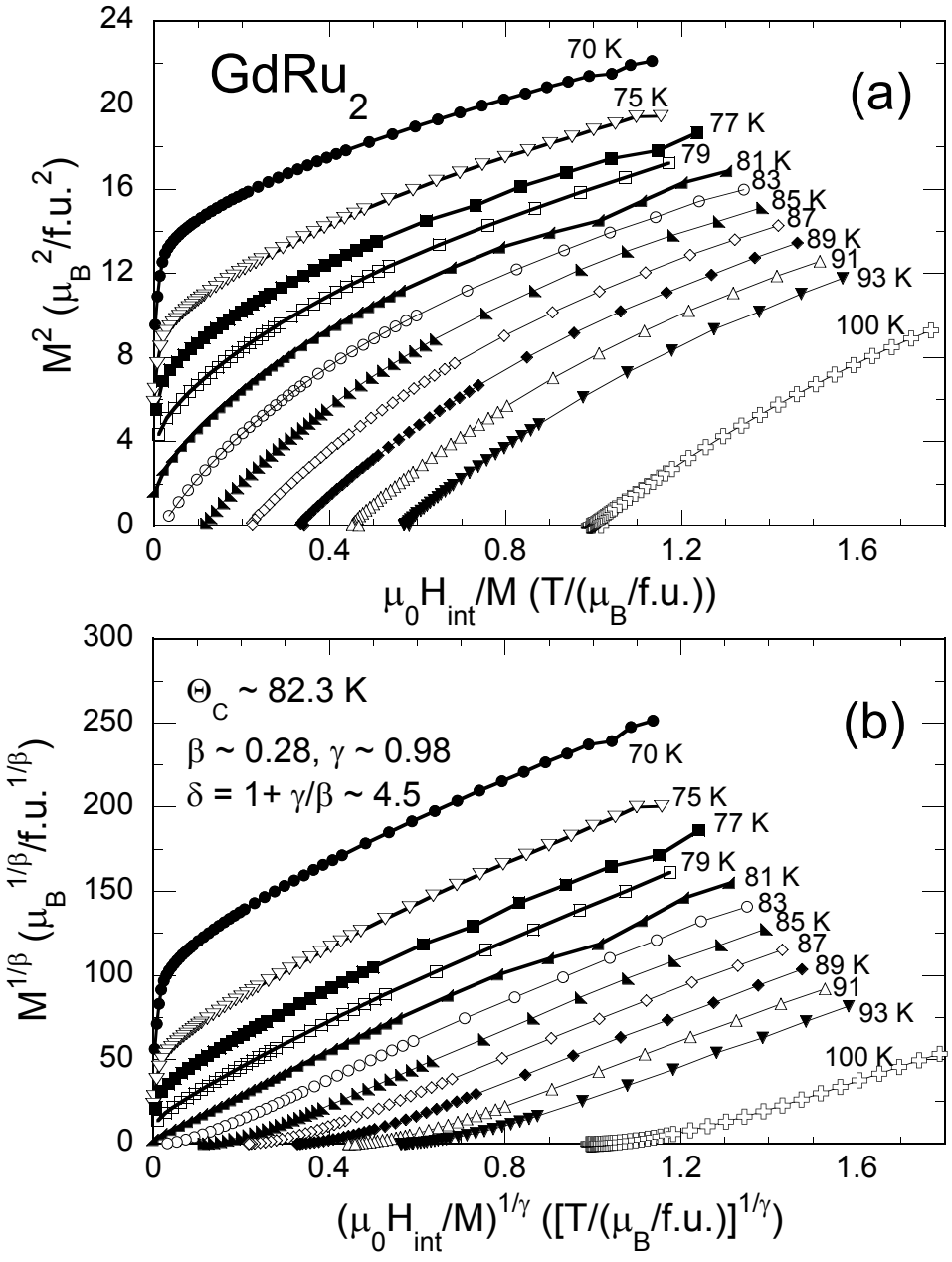

FIG. 3: (a) Conventional and (b) modified Arrott plots of $GdRu_2$. The Curie temperature T_C of $GdRu_2$ is ~ 82.3 K. The choice of exponents in (b) gives a closer to linear behavior in the critical region for intermediate fields.

This could be due to a temperature dependent Θ_D of $GdRu_2$ or our overestimate for the phonon contribution to the specific heat.

A $HoRu_2$ sample was synthesized so that magnetic order could also be investigated using

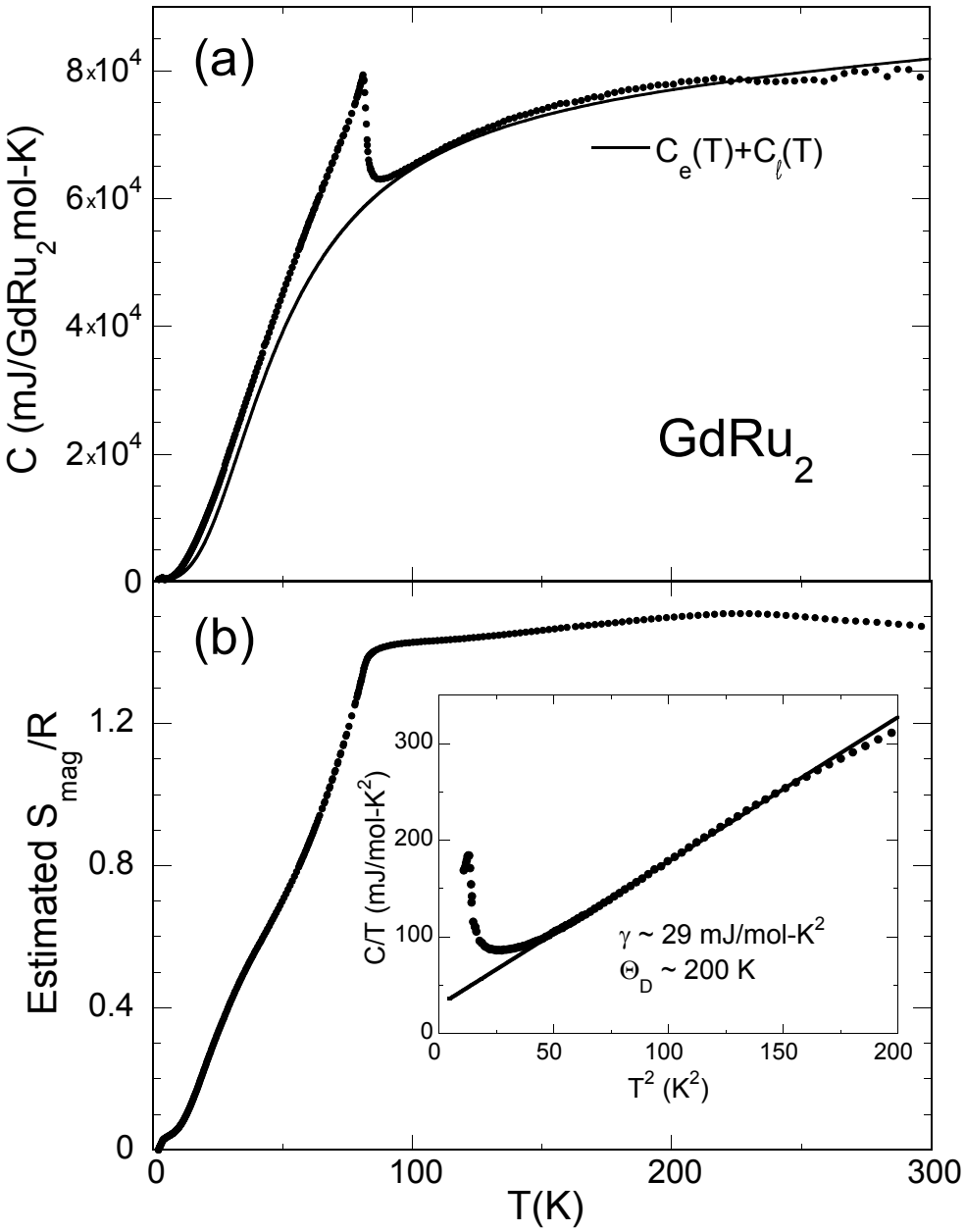

FIG. 4: (a) Specific heat C vs temperature T of $GdRu_2$. The solid line is the sum of the estimated contributions from band electrons and phonons $C_{\rm e}(T) + C_\ell(T)$. Inset of (b) C/T vs T^2 below 14 K. The estimated values of electronic specific heat coefficient γ and Debye temperature Θ_D are $\sim 29\,{\rm mJ/mol\text{-}}K^2$ and $\sim 200\,{\rm K}$, respectively. (b) Estimated magnetic entropy $S_{\rm mag}$ of $GdRu_2$ after the contributions from band electron and phonons is removed. The saturation value of $S_{\rm mag}$ is $\sim 1.5{\rm R}$, less than Rln8.

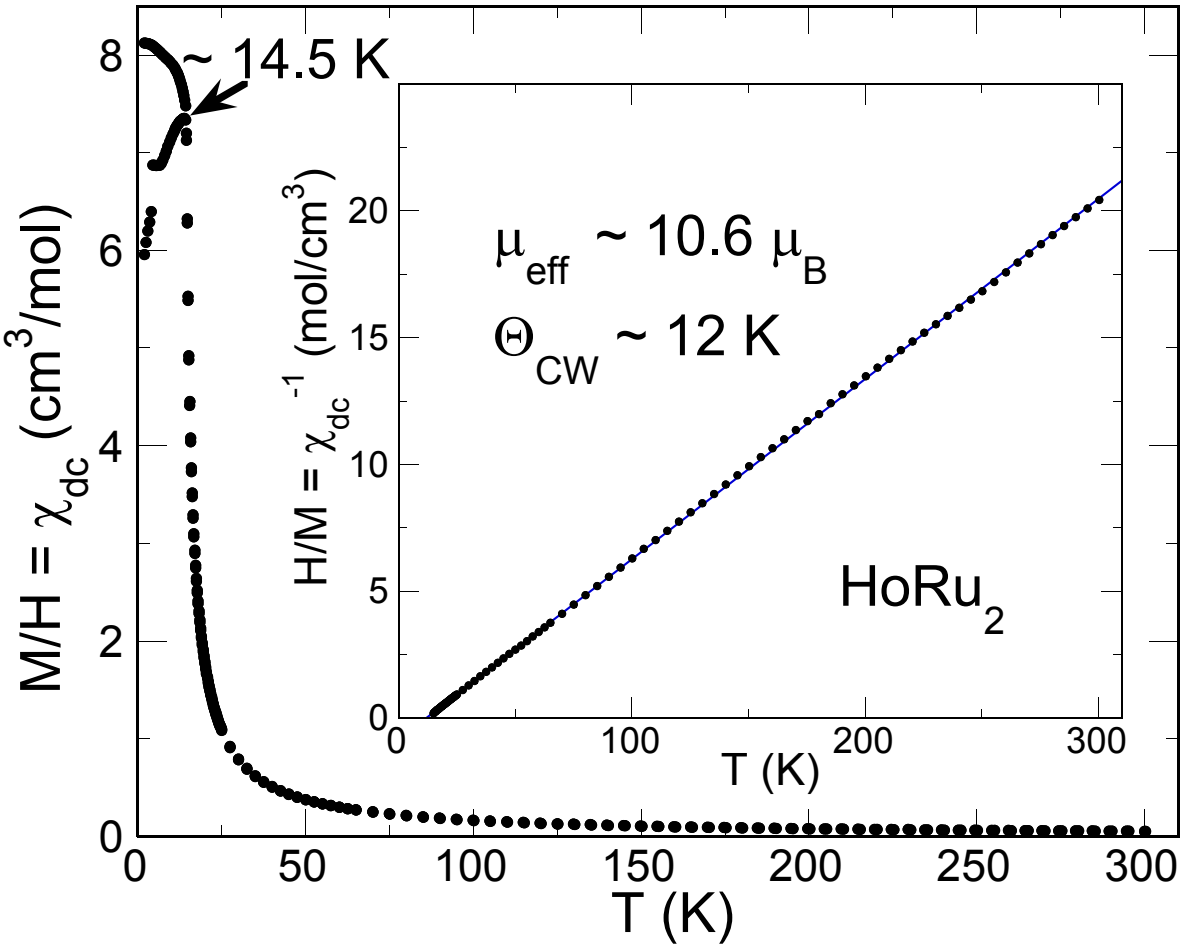

FIG. 5: Temperature dependence of dc-magnetic susceptibility $\chi_{\rm dc}$ of $HoRu_2$ measured at an applied magnetic field $H = 100\,$Oe. Hysteresis occurs at $T \sim 14.5\,$K. Inset $\chi_{\rm dc}^{-1}$ vs T fits well with a Curie-Weiss behavior, which results in an effective moment $\mu_{\rm eff} \sim 10.6\mu_{\rm B}$ and a Curie-Weiss temperature $\Theta_{\rm CW} \sim 12\,$K.

neutron diffraction. Gd has a large cross-section for neutron capture which makes investigations of $GdRu_2$ with neutron diffraction impractical. Measurements of $\chi_{\rm dc}$, performed on $HoRu_2$ at $H = 100\,$Oe and from 2 K to 300 K in the ZFC and FC conditions, are displayed in Fig. 5. Hysteresis in $\chi_{\rm dc}(T)$ occurs at $\sim 14.5\,$K. The Curie-Weiss analysis (shown in the inset of Fig. 5) indicates a ferromagnetic transition takes place near $\Theta_{\rm CW} \sim 12\,$K in $HoRu_2$ with a $\mu_{\rm eff} \approx 10.6\,\mu_B$, which agrees with the theoretical value $10.6\,\mu_B$ of the free ion moment of Ho^{3+}. An interesting feature in the ZFC $\chi_{\rm dc}$ data of $HoRu_2$ is that there is a 20% drop of the $\chi_{\rm dc}$ values at 2 K compared to the value at 14.5 K (similarly a $\sim 13\%$ drop in the ZFC $\chi_{\rm dc}$ of $GdRu_2$, Fig. 2).

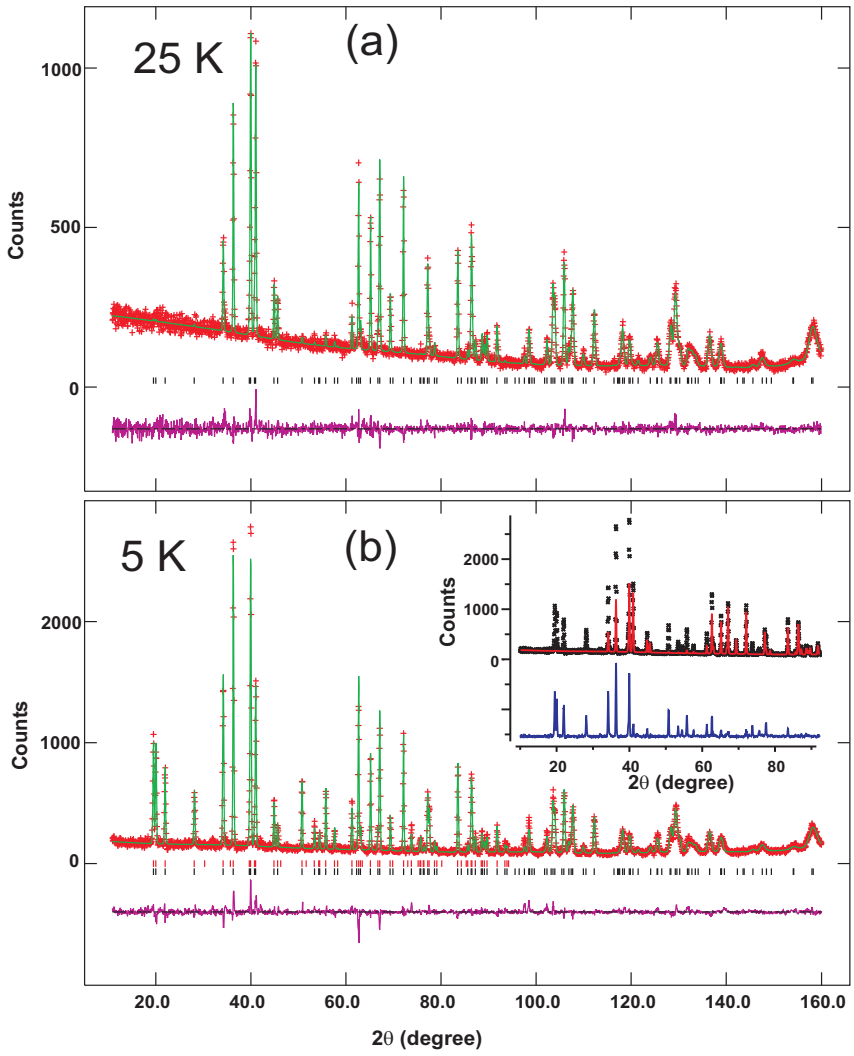

FIG. 6: (Color Online)High resolution neutron diffraction patterns taken (a) above and (b) below the magnetic phase transition at 15.3 K. The crosses indicate the observed data and the solid curves the calculated intensities from the structural refinements, and the difference is shown in the low part of the plots. The vertical lines indicate the angular positions of the diffraction lines for the nuclear Bragg peaks, and (b) for the magnetic (top) Bragg peaks.

TABLE I: Refined crystal structure parameters for $HoRu_2$ at 25 K (first line) and 5 K(second line) Space group *P6/3mmc*(No.194) a=5.2310(2)(Å), c=8.8265(4)(Å), V=209.16(2)(Å^3).

Atom	x	y	z	B(Å^2)	$M_x(\mu_B)$	$M_z(\mu_B)$	$M(\mu_B)$
Ho	1/3	2/3	0.0664(2)	0.36(3)			
	1/3	2/3	0.0660(2)	0.03(3)	6.70(8)	4.3(1)	7.98(8)
Ru_1	0	0	0	0.39(3)			
	0	0	0	0.22(3)			
Ru_2	0.1704(2)	0.3407(2)	3/4	0.39(3)			
	0.1711(2)	0.3422(4)	3/4	0.22(3)			
	Rp=6.16%,		*wRp*=7.34%,		χ^2=0.8387		
	7.12		9.02		1.428		

High resolution powder diffraction data were collected at the NCNR on the BT-1 high-resolution neutron powder diffractometer, using monochromatic neutrons of wavelength 1.5403Å produced by a Cu(311) monochromator. Söller collimations before and after the monochromator and after the sample were 15, 20, and 7 full-width-at-half-maximum (FWHM), respectively. Data were collected in the θ range of 3^o to 168^o with a step size of 0.05^o at 25K and 5K, above and below the magnetic phase transition. Structural refinements were carried out using the GSAS program.[35]

Detailed temperature dependent measurements of the magnetic order parameter were carried out on the BT9 triple axis spectrometer. A pyrolytic graphite (PG) (002) monochromator was employed to provide neutrons of wavelength 2.36 Å, and a PG filter was used to suppress higher-order wavelength contaminations. Coarse collimations of 40, 48, and 40 FWHM on BT9 were employed to maximize the intensity. A PG(002) energy analyzer was used in these measurements. Inelastic measurements were taken with a fixed final energy of 14.7 meV.

Fig. 6 shows the diffraction pattern obtained above (25K) and below (4 K) the magnetic transition. The diffuse background scattering in the magnetically disordered state is due to

paramagnetic scattering of the uncorrelated Ho moments, which decreases with increasing angle due to the magnetic form factor. The overall refinement fits at both temperatures are excellent. The structure is found to deviate slightly from the ideal phase, and the refined values for the crystal structure are given in Table 1. In the ground state the Ho ions exhibit long range ferromagnetic order, with both in-plane and c-axis components of the ordered moment also given in Table 1. We find an ordered moment of $7.98(8)\mu_B$, which is in good agreement with the low temperature magnetization data of Andoh[12] and somewhat smaller than the Curie-Weiss value obtained from the magnetization measurements. No evidence was found for moments on the Ru sites. The crystal and magnetic structures are shown in Fig. 7.

The temperature dependence of the magnetic Bragg intensity, which is proportional to the square of the ordered magnetic moment, is shown in Fig. 8. The temperature dependence is typical for magnetic ordering, and the solid curve is a least-squares fit of the intensity to a mean field order parameter, which provides a good fit to the data with a Curie temperature of 15.30(4) K.

The diffraction data indicate that the ordered moment is reduced from the free-ion value of $10.0\mu_B$, which suggests that crystal field effects are important in this system. We therefore carried out inelastic neutron scattering measurements on BT-7 for several temperatures and wave vectors to search for crystal field excitations. Figure 9 shows a scan above the phase transition, at a temperature of 20 K. We see two clear excitations from the crystal field ground state, a strong one at 2.83(5) meV and a weaker excitation at 14.82(5) meV. The energies and intensities turn out to be quite similar to the Ho crystal field levels observed in the closely related $Ce_{1-x}Ho_xRu_2$ system for smaller x[8, 9], which has the cubic C-15 Laves structure. The rare earth site symmetry in the $CeRu_2$ case is cubic, $\bar{4}3m$, and the crystal field level scheme has been worked out in detail. For hexagonal $HoRu_2$ the site symmetry is lower, $3m$, but the crystal field levels look remarkably similar nevertheless. The width for the higher energy level is limited by the instrumental resolution, while the level at 2.83 meV has an observed full-width-at-half-maximum (FWHM) of 4.34(12) meV, which is much broader than the resolution of 1.5 meV. The width likely originates from exchange broadening. We note that both excitations are clearly magnetic in origin, as their intensity decreases with increasing wave vector, following the magnetic form factor dependence, and they decrease

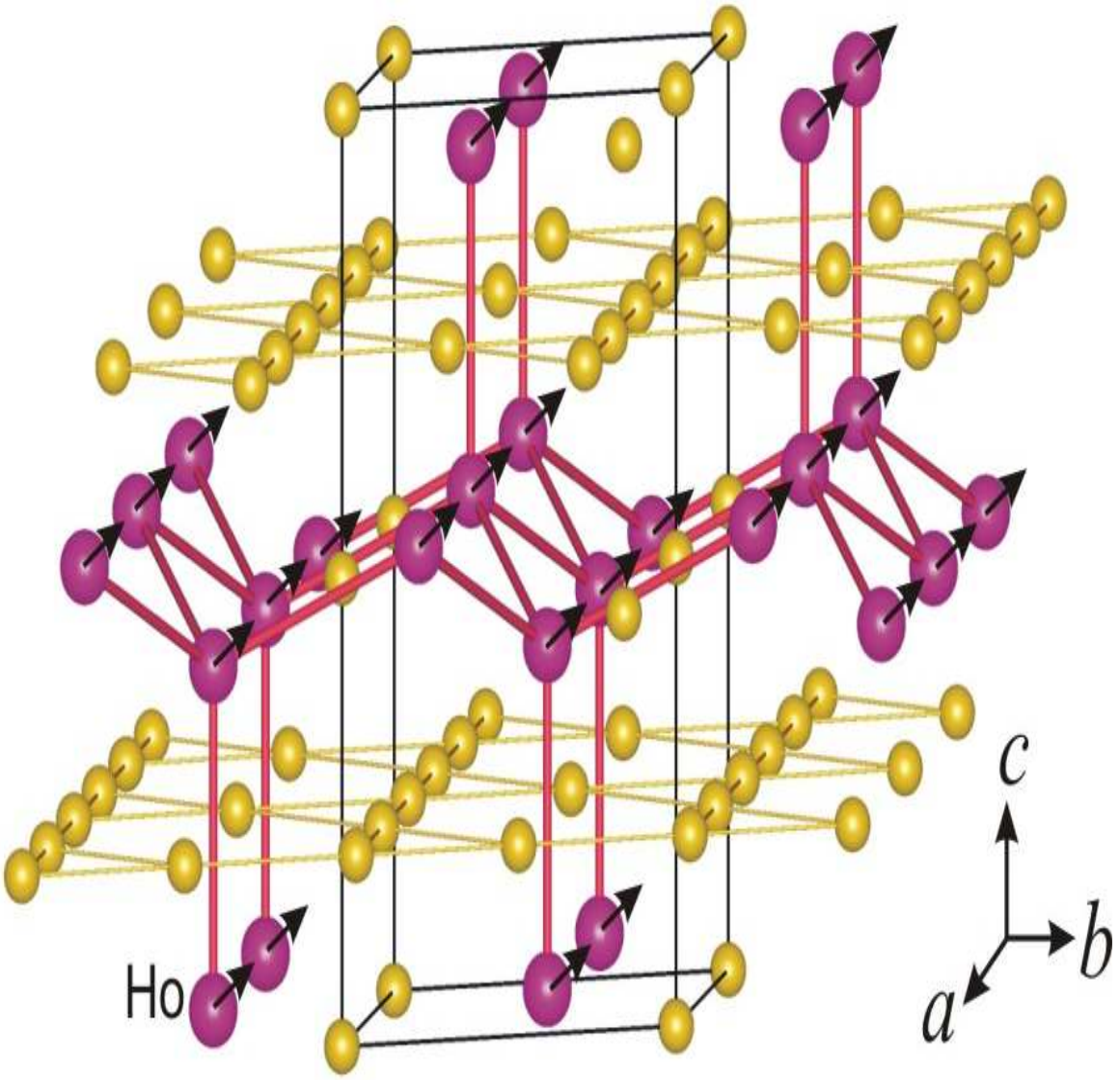

FIG. 7: (Color Online)The hexagonal laves phase and magnetic structure of $HoRu_2$ at 5 K. The ferromagnetically ordered moments on the Ho sites have a magnitude of $7.98(8)\mu_B$.

in intensity with increasing temperature as the ground state occupancy is depleted.

All the thermodynamic, transport, neutron diffraction measurements clearly demonstrate that ferromagnetic order develops in $GdRu_2$ below 83 K and in $HoRu_2$ below 15 K.

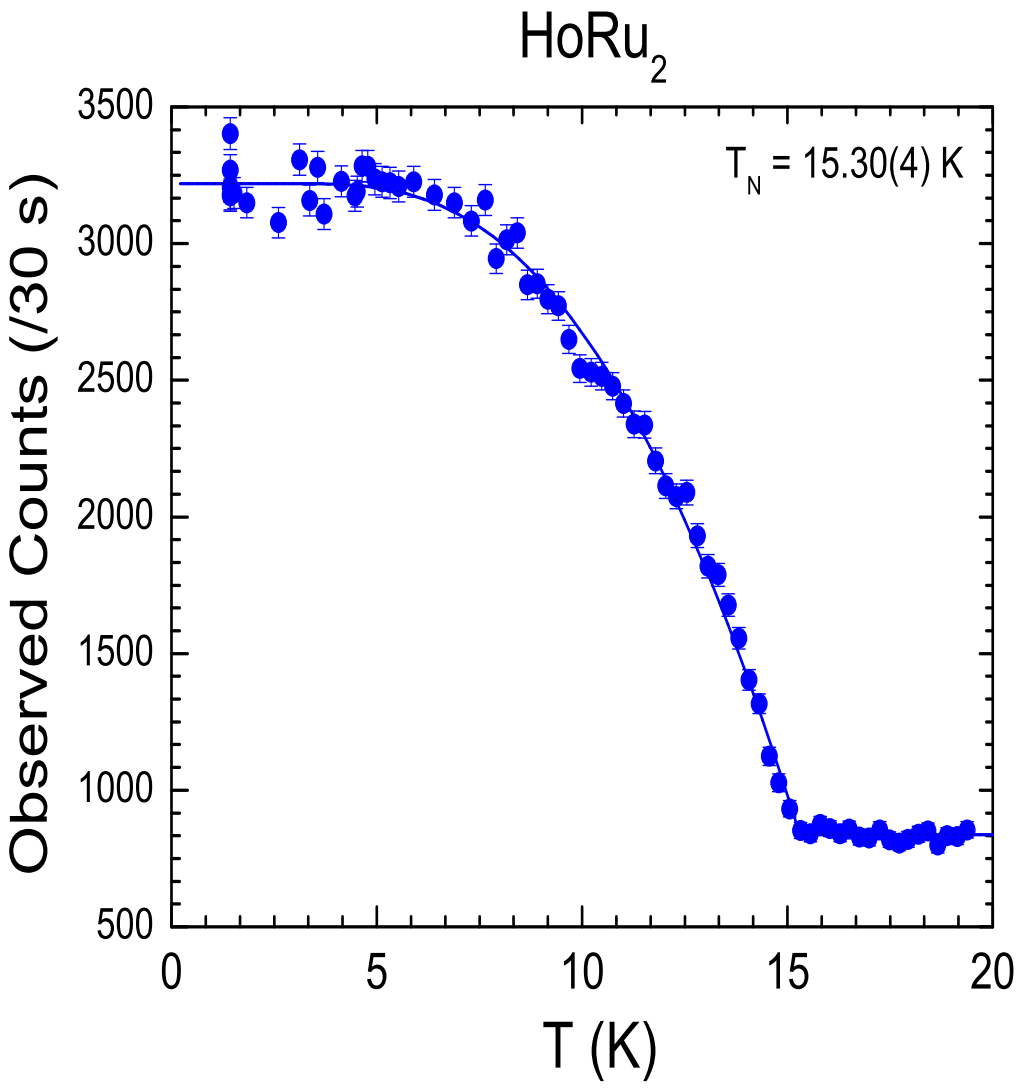

FIG. 8: (Color Online)Temperature dependence of the magnetic Bragg peak intensity, which yields an ordering temperature of 15.30(4) K. The intensity above the phase transition originates from the nuclear Bragg peak. Uncertainities are statistical in origin and represent one standard deviation.

B. ^{99}Ru Mössbauer Spectra

Details of the source preparation of ^{99}Rh(Ru), velocity calibration, and the experimental setup for transmission spectroscopy are discussed in previous papers[15, 16] The sample of $CeRu_2$ was made with natural Ru and contained 100mg/cm^2 of Ru. Samples of $GdRu_2$,

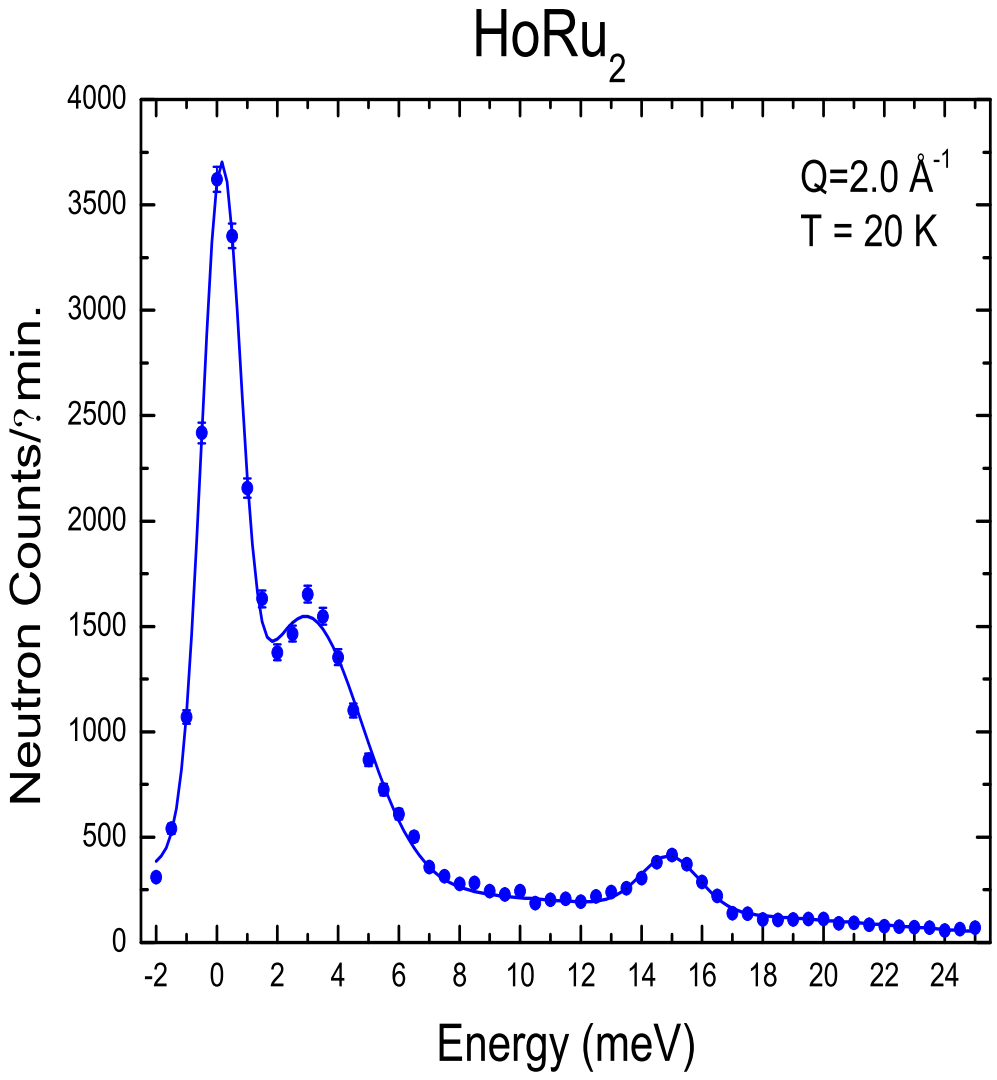

FIG. 9: (Color Online)Inelastic scattering observed at 20 K and a wave vector of 2.0 $Å^{-1}$. The elastic peak has a magnetic component and nuclear incoherent scattering, and is resolution limited. Two crystal field excitations are observed at 2.83(5) and 14.82(5) meV. The low energy scattering is broad, with a width of 4.34(12) meV. The energies and intensities are quite similar to the Ho crystal fields observed in cubic $Ce_{0.73}Ho_{0.27}Ru_2$[8, 9]

.

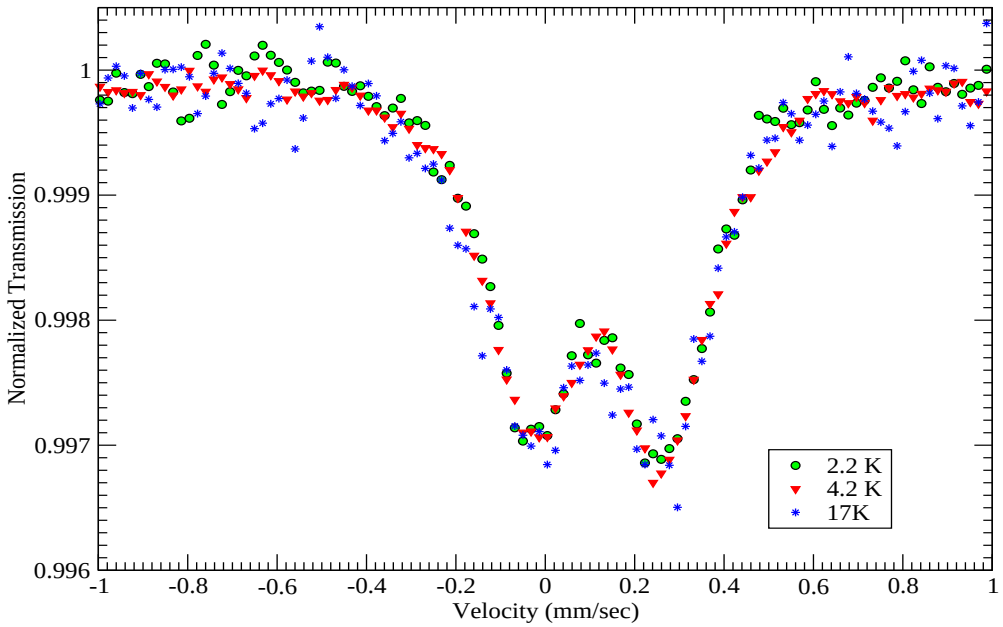

FIG. 10: (Color Online) ^{99}Ru Mössbauer spectra of $Ce_{0.88}Gd_{0.12}Ru_2$ at 2.2 K(o), 4.2 K($\bigtriangledown$), and 17 K($*$). Both the superconducting transition temperature and Curie temperature are $\sim$ 4 K[3]. The temperature independent spectra show no evidence of a hyperfine magnetic field.

$HoRu_2$, and $Ce_xGd_{1-x}Ru_2$ were prepared with enriched ^{99}Ru(95%). Typical samples contained about 65mg/cm^2 of ^{99}Ru. This made it possible to measure well-resolved spectra up to 150K. In the analysis of the spectra the number of inequivalent Ru sites is different in these materials. There is one type of Ru site in the unit cell of the cubic laves structure ($CeRu_2$), whereas there are two inequivalent Ru sites whose relative abundance is 1 to 3, in the hexagonal Laves structure ($GdRu_2$ and $HoRu_2$).

$CeRu_2$ is a superconductor with a transition temperature, T_{SC}, of 6K. As the Gd content of $Ce_xGd_{1-x}Ru_2$ increases with x, T_{SC} falls and goes to zero at $x \simeq 0.14$. Previous authors have suggested that superconductivity and ferromagnetism could coexist close to this doping level. The spectrum of $Ce_{0.88}Gd_{0.12}Ru_2$ at 2.2 K, 4.2 K and 17K is shown in Fig. 10. Extrapolating the data of Wilhelm and Hillebrand[3] gives values for T_{SC} and T_C both $\sim$4 K. There is no evidence in the temperature independent spectra for a hyperfine magnetic field, suggesting that ferromagnetism is ruled out at this doping. However, as doping with Gd increases, the low temperature phase is known to be ferromagnetically ordered and at

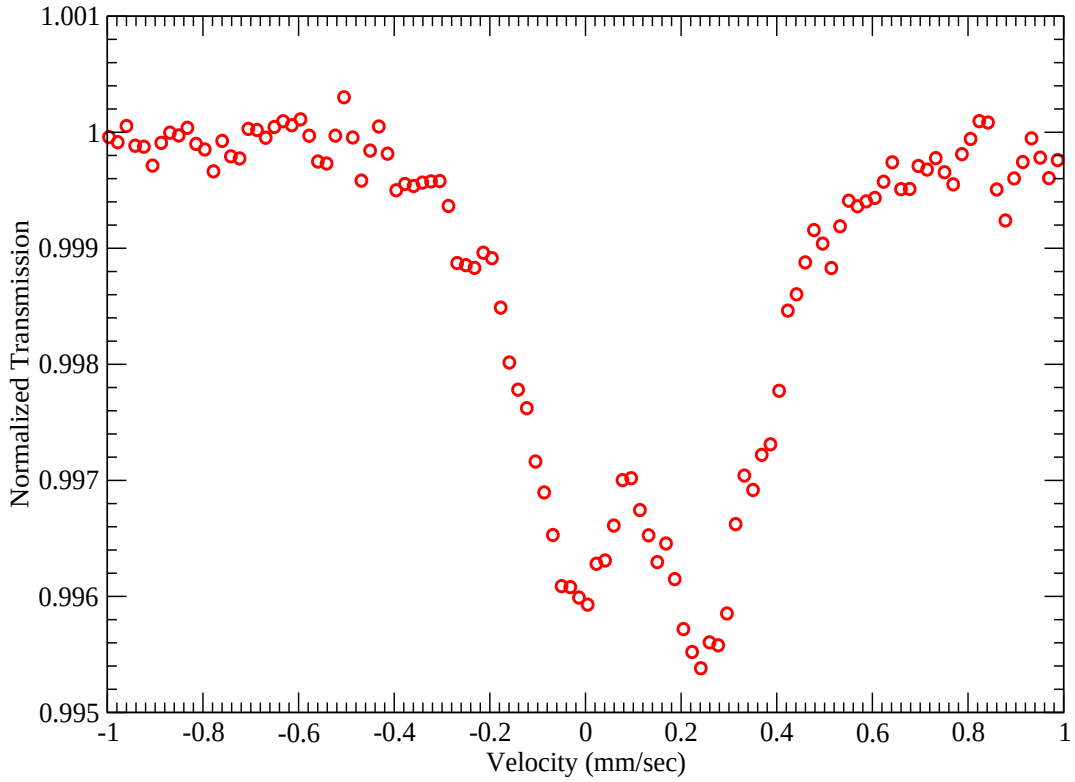

FIG. 11: (Color Online)^{99}Ru Mössbauer spectrum of $Ce_{0.2}Gd_{0.8}Ru_2$ at 4.2 K. Extrapolating the data of Wilhelm and Hillenbrand[3], T_C for this material is ∼60 K. This spectrum is very similar to that of $Ce_{0.88}Gd_{0.12}Ru_2$ except for additional asymmetry due to the increased Gd concentration. There is no evidence for the hyperfine magnetic field at the Ru site expected in a ferromagnetically ordered material.

$x = 0.2$ one would expect to see an eighteen line magnetic spectrum at 4.2 K due to a large value of $B_{hyperfine}$ field at the Ru site. Instead Fig. 11 shows a quadrupole spectrum which is somewhat more asymmetric than at x=0.88 due to the increased Gd content. The absence of hyperfine magnetic field even in this sample suggests that the spectra of $Ce_{0.88}Gd_{0.12}Ru_2$ do not rule out the coexistence of magnetism and superconductivity.

The Mössbauer spectrum for $GdRu_2$ is an almost temperature independent single peak between 4.2 K and 101 K except for a shift toward more positive velocities. This is shown

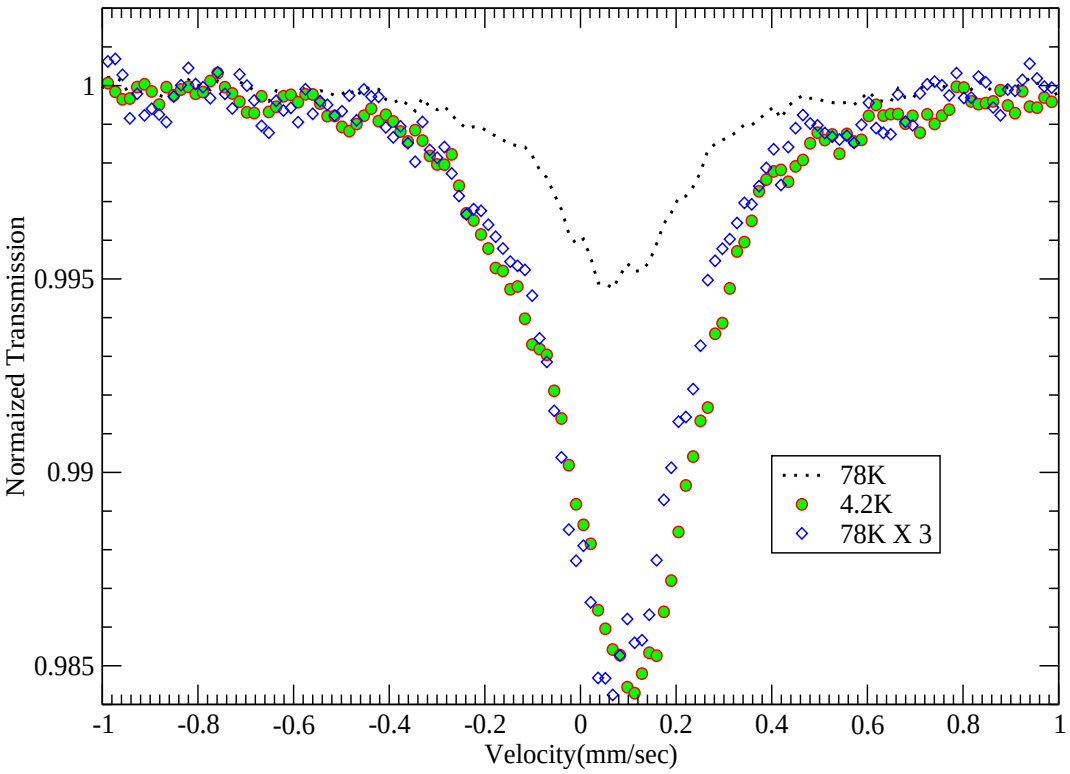

FIG. 12: (Color Online)^{99}Ru Mössbauer spectrum of $GdRu_2$ at 4.2 K (o) and at 78 K ($\diamond$) for a sample whose Curie temperature is 88.6 K. The 78 K spectrum(line) is scaled by 3.0 for direct comparison with the spectrum at 4.2 K. The only temperature dependence in the spectrum between 4.2 K and 100 K, based also on measured spectra at 89 K and 101 K, is a continuous shift of the isomer shift to slightly more positive values. Again there is no evidence of a hyperfine magnetic field.

in Fig. 12 for 4.2 K and 78 K, where the 78K spectrum is scaled by 3 to compensate for the temperature dependence of the recoil free fraction so that a direct comparison can be made with the 4.2 K spectrum. The experimental FWHM of the spectrum is slightly broader than that of Ru powder (0.25 mm/s). The width of the spectrum is unchanged with temperature. This is also the case for the spectra at 89 K and 101 K (not shown). Contrary to the transport, magnetic, and thermodynamic data on the same sample presented in the

previous section, there is no evidence of a transferred hyperfine field at the Ru sites due to magnetic order on the Gd sites.

The same apparent discrepancy between the Mössbauer spectrum and the experiments discussed above is seen in $HoRu_2$. The spectrum of $HoRu_2$ at 4.2 K is similar to that of $GdRu_2$. It is a single peak with no evidence of splitting due to a hyperfine magnetic field even though the temperature is far below the sample's Curie temperature, 15.3K. In order to get a more detailed picture of the properties of these materials we examined their electronic structure using *ab initio* calculations.

III. ELECTRONIC STRUCTURE

The lattice parameters and structure used in the calculations are those given by Compton and Matthias[1] for $CeRu_2$ and by the results of the neutron diffraction measurements of $HoRu_2$ at 5 K discussed. The lattice parameters and structure were measured by Compton and Matthias[1] for $GdRu_2$ at room temperature. However, the lattice frequently expands below a ferromagnetic transition in rare earth intermetallic compounds[36]. So we determined lattice constants for $GdRu_2$ at low temperatures by scaling the lattice constants given by Compton and Matthias and found that the total energy was minimised when their values were increased by $\sim 1\%$.

A. Density of States and Magnetic Order

The absence of the expected large splitting in the Mössbauer spectra in $GdRu_2$ and $HoRu_2$ points to a very small values of $B_{hyperfine}$ given that the materials are ferromagnetically ordered. This is completely different from the ruthenates where the dependence of the Mössbauer spectra reflect the internal ordered field.[15, 16] In particular, $SrRuO_3$ orders ferromagnetically at 163 K and the value of $B_{hyperfine}$ is found to be 33 T at 4.2 K.

We have calculated the electronic structure and the values of $B_{hyperfine}$ at the Ru and lanthanide sites using the Wien2k software package[28]. These calculations use the LSDA, which is implemented using an extension of the augmented plane wave(APW) method. Up to 729 inequivalent $\vec{k}$ points were used in the $P6_3/mmc$ structure and RKMAX was set at 8 to ensure convergence. The energy and charge convergence variables were $ec = 10^{-5}$

Rydbergs and $cc = 10^{-5}e$. In each region a wavefunction basis set is chosen to optimize the calculation. The spin on each site, S, is the net electronic spin polarization in the sphere surrounding that site.

The calculated contributions to the densities of states in $CeRu_2$, $GdRu_2$, and $HoRu_2$ show that the f-bands are narrow in each case, pointing to predominantly localized states. In $CeRu_2$ the calculated ground state is paramagnetic and the f-band is mostly above the Fermi energy, with small weight at E_F so that the f electrons also contribute to the conduction band. This is in agreement with the earlier *ab initio* calculations of Yanase[37] and Higuchi and Hasegawa[38] and with experiment.

The calculated contributions to the density of states of $GdRu_2$ from the Gd $4f$ band and from the $4d$ bands associated with the two inequivalent Ru sites sites are shown in Fig. 13. The Gd spin up f-band is $\sim$4 eV below the Fermi level and spin down f-band is $\sim$1.5 eV above. The calculated value of net spin, S, on the Gd sites is 3.46 which is very close to the Hund's rule result for Gd, $\frac{7}{2}$, and to the result of the Curie-Weiss fit to the magnetic susceptibility. The calculated values of S at the two inequivalent Ru sites in $GdRu_2$ are very small, $\sim$-0.06 and $\sim$-0.09. The bottom two panels in Fig. 13 show the contributions to the density of states from Ru $4d$ electrons at the two inequivalent Ru sites. $N_\uparrow$ is the contribution for states with spin parallel to the moment of the Gd site and is positive, and the contribution from spin down, $N_\downarrow$, is negative for each of the inequivalent Ru two sites. At the Fermi energy the density of states is dominated by the Ru $4d$ electrons, which form broad conduction bands. The contributions from Ru $4d$-electrons, $N_\uparrow$ and $N_\downarrow$, and $N_\uparrow - N_\downarrow$ are plotted in Fig. 14 in the energy range which is $\sim$0.1 eV on either side of the Fermi energy, E_F=0. It is seen that the d-electrons from both Ru sites are polarized parallel to the Gd moment with $\frac{N_\uparrow - N_\downarrow}{N_\uparrow + N_\downarrow} \simeq 0.2$ for each band arising from the two inequivalent Ru sites. The total Ru d density of states $\sim$1.0 $(\text{eVRu})^{-1}$ at E=E_F.

On the other hand the Gd s-electrons have negligible weight at E_F, $\simeq$0.02 $(\text{eVGd})^{-1}$ and are unpolarized. This is also the case for Ru s-electrons. This suggests that Ru d-electrons mediate the interaction between localized Gd f-moments. In $HoRu_2$, the Ru $4d$ Ru electrons play the same role but the minority spin band is at the Fermi energy so that it is partially occupied.

In $HoRu_2$, the value of S at the Ho site is $\simeq$1.82. This value of S is slightly lower than 2, the value consistent with the effective moment given by the fit to magnetic susceptibility,

as determined by Hund's Rules. The absence of moments on the Ru sites in $HoRu_2$, S$\simeq$0, is consistent with the neutron diffraction data.

According to these results, the magnetic properties can be described by a model in which localized Gd or Ho f-moments couple to itinerant Ru d-electrons, rather than to itinerant s electrons[24].

B. Hyperfine Magnetic Fields and Electric Field Gradients

$B_{hyperfine}$ at a given site has a number of contributions which have been derived with relativistic corrections by Blügel et al.[39] and can be calculated directly using the Wien2k package[40]. These contributions are B_{con}=B_{core}+$B_{valence}$, the Fermi contact term, B_{dip}, the dipolar field from the on-site spin density, B_{orb}, the field associated with the on-site orbital moment, and B_{lat} , the classical dipolar field from all other atoms in the system carrying moments. B_{core} is the contribution due to polarization of core electrons and $B_{valence}$ is the contribution from the polarization of the valence or conduction band electrons. These are by far the largest contributions. Powder samples are used in the experiments with small crystallites so that each Ru nucleus sees the average of a collection of randomly orientated dipolar fields which presumably sum to zero. Therefore, we take B_{lat} to be zero in the current analysis.

The calculated $B_{hyperfine}$ and local moments at the Ce and Ru sites in $CeRu_2$ are essentially zero, consistent with the absence of magnetic order. The calculated contributions to $B_{hyperfine}$ are shown in Table 2 for $GdRu_2$ and in Table 3 for $HoRu_2$. The values of $B_{hyperfine}$ at the Ru sites are surprisingly small compared to that at the rare earth sites in both compounds, consistent with the Mössbauer data. By comparison, the transferred hyperfine field at the Ir site in $Ir_{0.01}Fe_{0.99}$ is 14.3 T compared to 32 T at the Fe site[20]. The different contributions to $B_{hyperfine}$ on the Ru sites are all small, leading to modest values for $B_{hyperfine}$. The values of $B_{hyperfine}$ at the Ru nuclei are sensitive to the value of the lattice constants. In order to determine the lattice constants for $GdRu_2$ at low temperature, the electronic properties were calculated for values of the lattice constants given by Compton and Matthias[1] scaled by a common factor, α, from 0.995 to 1.05. Although the value of the net spin on the Gd site did not change for this range of lattice constants, the hyperfine magnetic fields at the Ru sites varied from -4.49 T at $\alpha = 1.00$ to 0.1 T at $\alpha = 1.05$. The

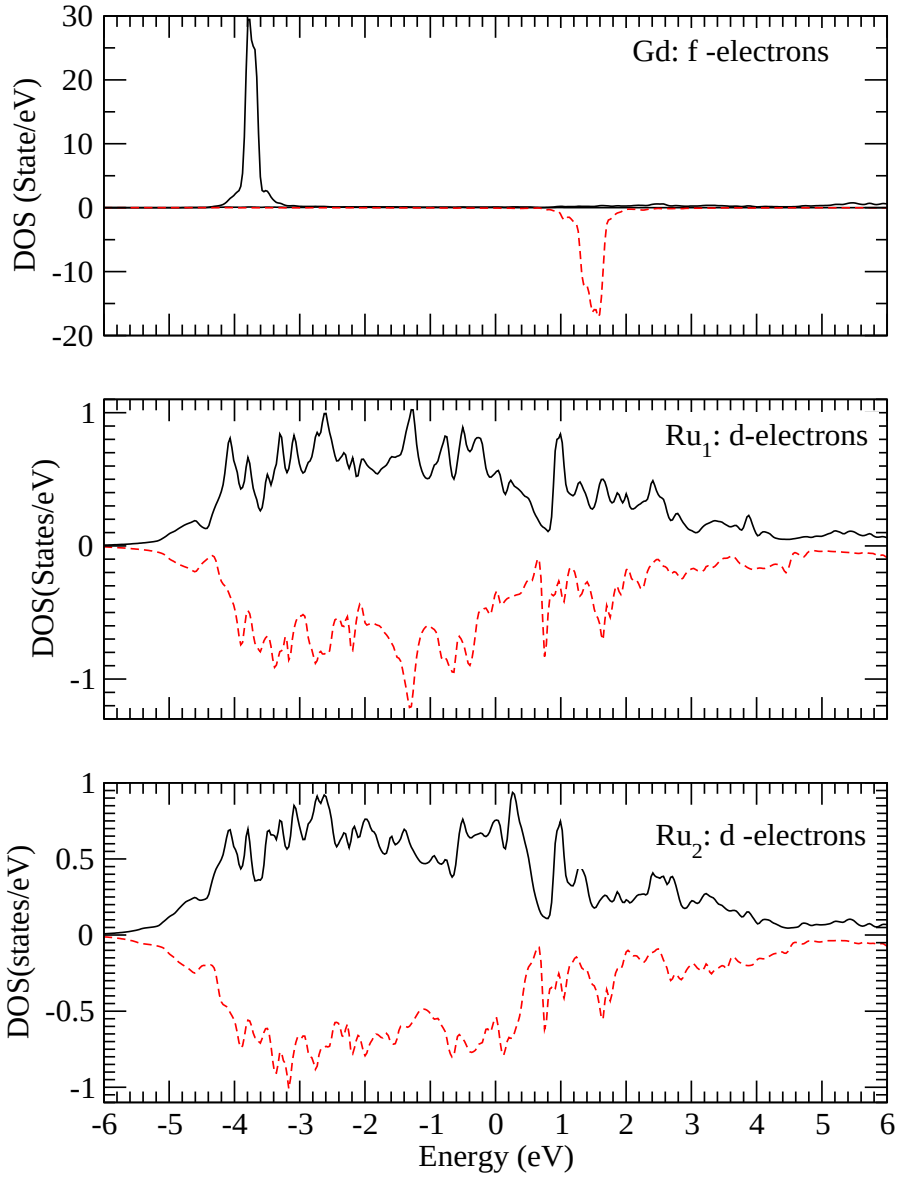

FIG. 13: (Color Online) Contributions to the Density of States in $GdRu_2$. Lines are spin up and dashed-lines are spin down. E=0 is the Fermi level.

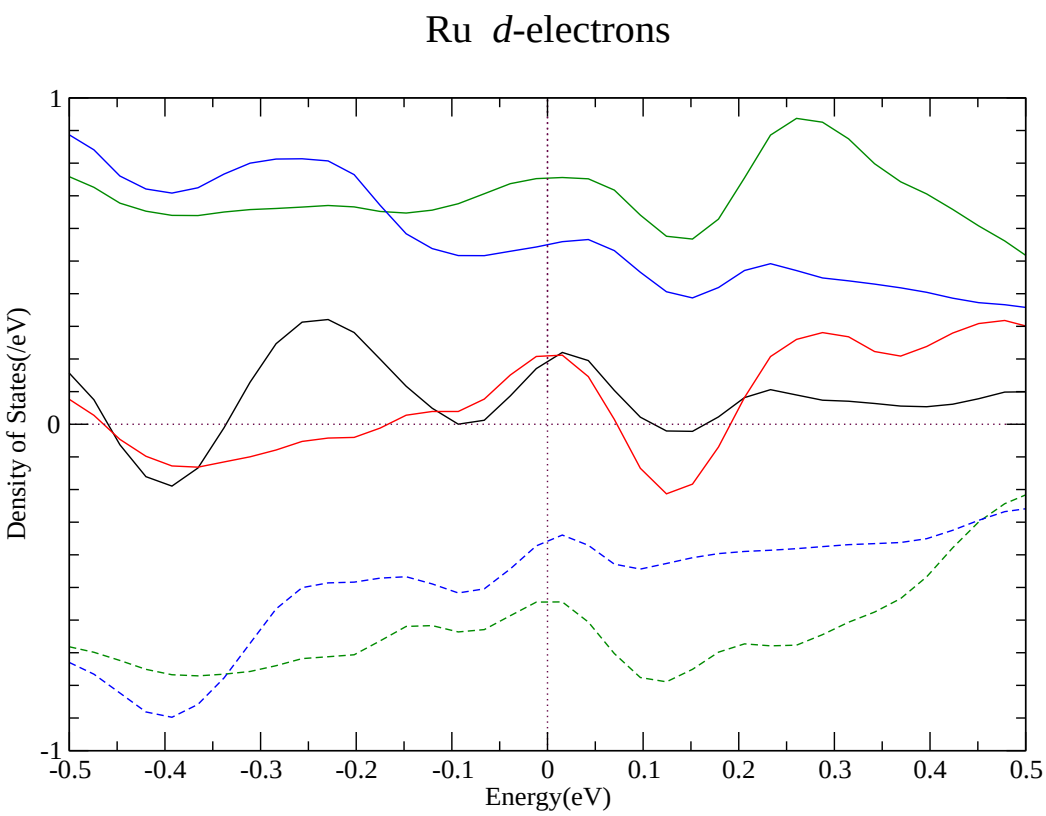

FIG. 14: (Color Online) Polarization of d-electrons from the two inequivalent Ru sites. Black line - $N_\uparrow - N_\downarrow$ from Ru site-1. Red line - $N_\uparrow - N_\downarrow$ from Ru site-2. Blue and green lines above zero line are spin up and the corresponding dashed-lines below the zero line are spin down. E=0 is the Fermi level.

lowest total energy for a formula unit occurs at $\alpha = 1.01$ and the values for $GdRu_2$ are calculated with this α. From Table 2, $B_{hyperfine}$ at both Ru sites is negative, as one would expect from transferred hyperfine fields[22, 23].

Examining the contributions to $B_{hyperfine}$ on the rare earth site one sees that B_{core} and $B_{valence}$ are large and of opposite sign. This is again consistent with the original discussion of Watson and Freeman[22, 23]. The other contributions are negligible by comparison in $GdRu_2$. However, in the $HoRu_2$ site B_{orb} ~40 T, is a substantial fraction of $B_{hyperfine}$ on the Ho site due to the almost complete cancellation of the B_{core} and $B_{valence}$. This difference in the value of B_{orb} at the Gd and Ho sites is a reflection of the difference in the orbital angular

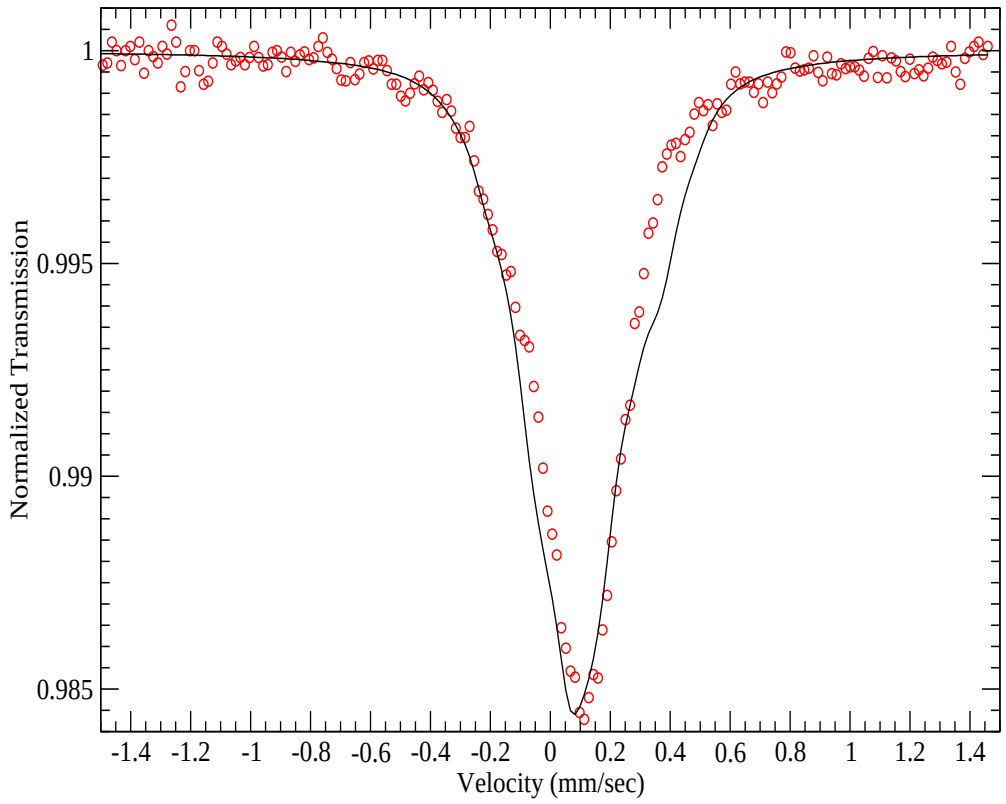

FIG. 15: (Color Online)Mössbauer spectrum of $GdRu_2$ at 4.2 K (o) for a sample whose Curie temperature is 83.2 K. The solid line is the spectrum calculated with the electric field gradient components and the $B_{hyperfine}$, shown in Table 2 and 4. The fitting parameters are the isomer shifts at the two inequivalent Ru sites, IS_1=0.0 mm/sec and IS_2=0.12 mm/sec, and the half-width of the lines, Γ=0.07 mm/sec.

momentum quantum number, L, on the Gd and Ho sites. Whereas Hunds' rules give $L = 0$ on the Gd site because of the half-filled $4f$ shell, they give $L = 6$ on the Ho site.

The calculated components of the EFG tensor for $CeRu_2$, $GdRu_2$, and $HoRu_2$ are given in Table 3. Since the Ce site symmetry is cubic the electric field gradient is zero. The components of the EFG at the Ru site, V_{xx}=V_{yy}=2.80×10^{21}Vm^{-2}, are small compared to those in RuO_2[27], which also has a pure quadrupole spectrum, suggesting that the Ru sites have almost cubic symmetry. In $GdRu_2$ and $HoRu_2$, the EFG are different at the two inequivalent Ru sites. Again the magnitude of the components of the EFG suggests that there is almost cubic symmetry at these sites.

The Mössbauer spectra for these materials can now be almost completely determined

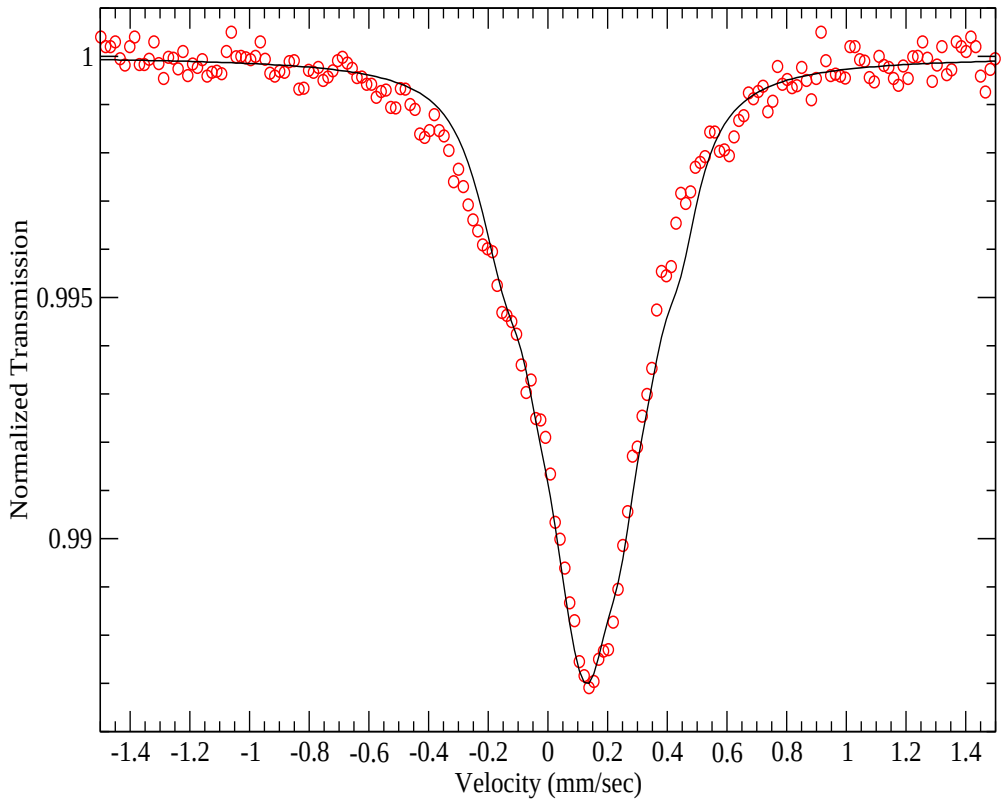

FIG. 16: (Color online) ^{99}Ru Mössbauer spectrum of $HoRu_2$ at 4.2 K. The Curie temperature is 15.3 K for this sample. The solid line is the spectrum calculated with the electric field gradient components and the $B_{hyperfine}$, shown in Table 2 and 4. The fitting parameters are the isomer shifts at the two inequivalent Ru sites, IS_1=0.05 mm/sec and IS_2=0.18 mm/sec, and the half-width of the lines, Γ=0.08 mm/sec.

with these calculated hyperfine magnetic fields and electric field gradients. The additional parameters are the half-width half-maximum, Γ, of the absorption lines and the isomer shifts at the Ru sites. These are choosen to fit the data. The $GdRu_2$ spectrum at 4.2 K is shown in Figure 15 and that of $HoRu_2$ in Figure 16. The line through the spectrum is determined by the EFG tensor and values of $B_{hyperfine}$ at the two inequivalent Ru sites calculated with the parameters in Table 1, Table 2, and Table 3. The non-Lorenzian shape is due to the calculated difference in the EFG's at the two sites.

In Figure 17 we show the Mössbauer spectrum of $CeRu_2$ at the Ru site at 4.2 K. The full line is the spectrum determined with values of the electric field gradient tensor (EFG) at the Ru site in Table 3. Other parameters in these spectra are the isomer shift, IS=0.12

TABLE II: $GdRu_2$: Net electron spin, S, and contributions to the hyperfine magnetic fields(T) at the Gd and Ru sites

	S	B_{core}	$B_{valence}$	B_{orb}	B_{dip}	$B_{hyperfine}$
Gd	3.46	334.55	-285.51	-2.88	-.29	49.05
Ru_1	-0.06	-4.83	0.63	-.08	0.01	-4.20
Ru_2	-0.09	-3.78	1.06	-.0.20	0.05	-2.72

TABLE III: $HoRu_2$: Net electron spin, S, and contributions to the hyperfine magnetic fields(T) at the Ho and Ru sites

	S	B_{core}	$B_{valence}$	B_{orb}	B_{dip}	$B_{hyperfine}$
Ho	1.82	179.32	-161.31	38.72	-.41	56.34
Ru_1	0.028	-1.63	-0.26	-0.02	0.01	-1.90
Ru_2	-0.009	-2.61	0.69	-0.75	-0.070	-2.74

mm/sec, and the half-width of lines, Γ=0.11 mm/sec.

The calculations discussed here have demonstrated that it is possible for transferred hyperfine magnetic fields at the Ru sites to be very small in these ferromagnetic materials and allow us to reconcile the apparent contradiction between the results of the ^{99}Ru ME measurements and those of the transport, magnetic susceptibility, magnetization, and neutron diffraction experiments on $GdRu_2$ and $HoRu_2$.

TABLE IV: Diagonal elements of the Electric field gradient tensor (10^{21}V/m^2) at different sites in $GdRu_2$ and $HoRu_2$.

Ce	(0.,0.,0.)		Gd	(-1.40,-1.40,2.79)		Ho	(-1.34,-1.34,2.68)
Ru	(2.80,2.80,-5.60)		Ru_1	(3.42,3.42,-6.83)		Ru_1	(3.85,3.85,-7.71)
			Ru_2	(1.86,0.90,-2.76)		Ru_2	(1.30,0.90,-2.19)

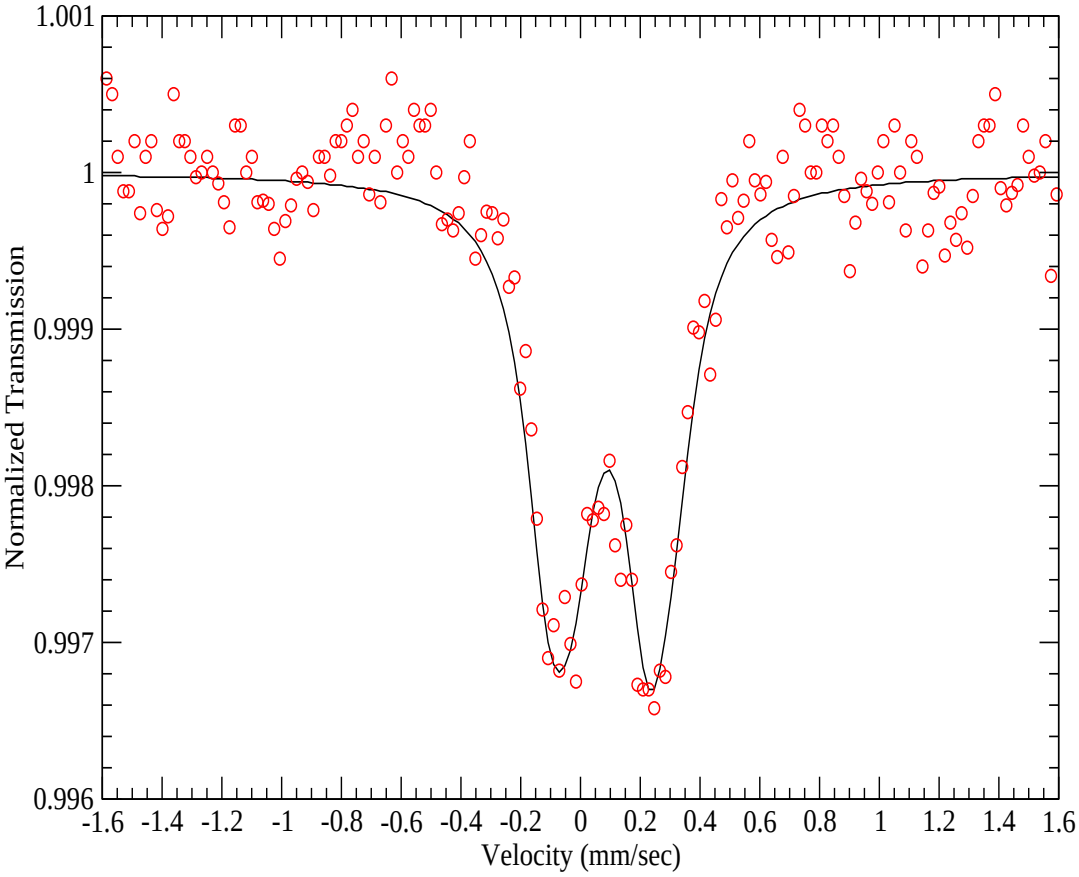

FIG. 17: (Color Online) ^{99}Ru Mössbauer spectra of $CeRu_2$ at 4.2 K(o). The line is the spectrum determined by the calculated EFG's, Table 3, using 0.09 mm sec^{-1} as the full-width half-maximum and isomer shift equal to 0.09 msec^{-1}.

IV. DISCUSSION

A basic assumption of using the ^{99}Ru ME is that the spectrum reflects the electronic environment in the material and that magnetic order is reflected in an induced hyperfine field. However the transferred hyperfine magnetic fields in ferromagnetic $GdRu_2$ and $HoRu_2$ are so small that one would conclude that these materials do not have magnetic order. The calculated properties of these materials have shown how this apparent discrepancy between

Mössbauer, the collapse of the hyperfine magnetic field, and results of neutron diffraction, magnetization, transport and specific measurements on the same samples arise. Analyzing the calculated contributions to $B_{hyperfine}$, the net electronic spin, S, on the Gd and Ho in Tables 1 and 2 is roughly proportional to the magnitude of the largest contributions, B_{core} and $B_{valence}$. This suggests that $B_{hyperfine}$ is $\simeq 0$ on the Ru sites because S is $\simeq 0$ on these sites. This arises because $4d$ Ru electrons form polarized conduction bands rather than localized moments. Consequently the ^{99}Ru ME is misleading regarding magnetic order in the RRu_2 intermetallics.

In contrast, moments in the magnetically ordered ruthenates are shared between Ru and O sites[41, 42] and the temperature dependence of magnetic order is reflected in $B_{hyperfine}$ determined from the Mössbauer spectra. The $2p$ orbitals of the six neighboring oxygen atoms in the RuO octahedra are strongly hybridized with Ru $4d$ electrons. A possibile explanation for the different behavior of Ru in the ruthenates and intermetallics lies in the difference in the electronegativities between Ru and O compared to that between Ru and rare earth atoms. The Pauling electronegativity of oxygen atoms is 3.44, which is larger than that of Ru(2.2)[43]. In $GdRu_2$ and $HoRu_2$, the opposite is the case. For Gd and Ho, the electronegativity values are 1.1 to 1.25. As a result the rare-earth atoms lose their $5d$ and two $6s$ electrons which take on the character of Ru d electrons. Competition for electrons between Ru atoms leads to the wide d-bands seen in the bandstucture. The structure can be pictured as a lattice of positive Gd and Ru ions, with the $4f$ moments tightly-bound on the rare-earth sites as in the rare-earth metals[44]. The $4d$ derived conduction bands mediate the coupling between the rare earth moments rather than forming localized moments on the Ru sites.

There seem to be few other examples where hyperfine magnetic fields have not been induced by magnetic order. There is evidence for a collapse of $B_{hyperfine}$ in hexagonal close-packed (hcp) Fe, which is the stable phase at high pressures. Whereas there is evidence that this phase is antiferromagnetically ordered from Raman scattering, the six-line ^{57}Fe Mössbauer spectrum disappears at the transition from bcc Fe to hcp Fe with increasing pressure[45]. $B_{hyperfine}$ was calculated by Seinle-Neumann et al.[46] also using the wien2k software. They found that there was almost complete cancellation of the large core and valence contributions to B_{con} as the atomic volume was reduced, simulating increasing pressure. In determining the lattice constants for $GdRu_2$ at low temperature, we also found that

the sign of $B_{hyperfine}$ changed as the lattice constants were varied, although not at the values of interest. However, the contributions to $B_{hyperfine}$ in $GdRu_2$ and $HoRu_2$ are less than 6 T due to the itinerant nature of the $4d$ electrons.

The results of this investigation point to the unsuspected sensitivity of a nuclear probe, such as the Mössbauer Effect, to the details of the electronic structure in magnetically ordered materials. The *ab initio* calculations provide a quantitative description of how the collapse of the hyperfine magnetic field at the Ru site arises. In doing so, it was shown that the Mössbauer spectrum can be a probe of bandstructure, as well as the local electronic environment.

V. ACKNOWLEDGMENTS

Work was supported by the USDOE(DE-FG02-03ER46064), by CCSA#7669 at CSU-Fresno, and by USDOE(DE-GF02-04ER46105), and NSF(DMR0802478), at UCSD. D. C. wishes to thank Dr. M. D. Jones of the Center for Computational Research at the University of Buffalo for his help in using the Wien2k package.

[1] V. B. Compton, and B. T. Matthias, Acta Cryst. **12**, 651 (1959).

[2] B. T. Matthias, H. Suhl, and E. Corenzwit, Phys. Rev. Lett. **1**, 449 (1958).

[3] M. Wilhelm and B. Hillebrand, Physica **55**, 608 (1971).

[4] K. Ruebenbauer, J. Fink, H. Schmidt, G. Czjek, and K. Tomala, Phys. Stat. Sol. **84**, 611 (1977).

[5] K. Kumagai, T. Matsuhira, and K. Asayama, J. Phys. Soc. Jpn **45**, 422 (1978).

[6] Ø. Fischer and M. Peter in *Magnetism: A Treatise on Modern Theory and Materials*, volume V, edited by H. Suhl (Academic Press, New York and London, 1973), page 327.

[7] M. Peter, P. Donzé, Ø. Fischer, A. Junod, J. Ortelli, A. Treyvaud, E. Walker, M. Wilhelm and B. Hillenbrand, Helv. Phys. Acta **44**, 345 (1971).

[8] J. W. Lynn and C. J. Glinka, J. Mag. and Mag. Materials **14**, 179 (1979).

[9] J.W. Lynn, D. E. Moncton, L. Passell, and W. Thomlinson, Phys. Rev. B **21**, 70 (1980).

[10] J. O. Willis, D. J. Erickson, C. E. Olsen, and R. D. Taylor, Phys. Rev. **21**, 79 (1980).

[11] R. E. Watson and L. H. Bennett, Phys.Rev. B **15**, 502 (1977).

[12] Y. Andoh, J. Phys. Soc. Jpn **56**, 4075 (1987).

[13] A. Huxley, J. X. Boucherle, M. Bonnet, F. Bourdarot, I. Schustler, D. Caplan, E. Lelievre, N. Bernhoeft, P. Lejay, and B. Gillon, J. Phys. Condens. Matter **9**, 4185 (1997).

[14] P. I. Kripyakevich, V. F. Terekhova, O. S. Zarechnyuk, and I. V. Burov, Soviet-Crystallography **8**, 268 (1963).

[15] M. DeMarco, G. Cao, J. E. Crow, D. Coffey, S. Toorongian, M. Haka and J. Fridmann, Phys. Rev. B **62**, 14297 (2000).

[16] D. Coffey, M. DeMarco, B. Dabrowski, S. Kolesnik, S. Toorongian, and M. Haka, Phys. Rev. B **77**, 214412 (2008).

[17] G. K. Wertheim and J. H. Wernick, Phys. Rev. **125**, 1937 (1962).

[18] U. Atzmony, M. P. Dariel, E. R. Bauminger, D. Lebenbaum, I. Nowik, and S. Ofer, Phys. Rev. B **7**, 4220 (1973).

[19] H. de Graaf, R. C. Thiel, and K. H. J. Buschow, J. Phys. f: Met. Phys. **12** 1239 (1982).

[20] U. Atzmony, E. R. Bauminger, D. Lebenbaum, A. Mustchi, and S. Ofer, Phys. Rev. **163**, 314 (1967).

[21] D. Bosch, F. Pobell, and P. Kienle, Physics Letters **22**, 262 (1966).

[22] R. E. Watson and A. J. Freeman, Phys. Rev. Lett. **6**, 277 (1961).

[23] R. E. Watson and A. J. Freeman, Phys. Rev. **123**, 2027 (1961).

[24] B. D. Dunlap, I. Nowik, and P. M. Levy, Phys. Rev. B **7**, 4232 (1973).

[25] J. Callaway and C. S. Wang, Phys. Rev. B **16**, 2095 (1977).

[26] C. S. Wang and J. Callaway, Phys. Rev. B **15**, 298 (1977).

[27] O. C. Kistner, Phys. Rev. **144**, 1022 (1966).

[28] P. Blaha, K. Schwarz, G. K. H. Madsen, Kvasicka and J. Lutz, wien2k:*Augmented Plane Wave + Local orbitals Program for Calculating Crystal Properties*, (2001), (Technische Universität Wien, Wien, Austria).

[29] P. E. Lippens, J. Olivier-Fourcade, and J. C. Jumas, Hyperfine Interactions **126**, 137 (2000).

[30] P. Blaha, K. Schwarz, W. Faber, and J. Luitz, Hyperfine Interactions **126**, 389 (2000).

[31] J. Belošević-Čavor, N. Novaković, B. Cekić, N. Ivanović, and M. Manasijević, J. Mag. Mag. Mat. **272-276**, 762 (2004).

[32] E. Pavarini and I. I. Mazin, Phys. Rev. B **74**, 035115 (2006); Phys. Rev. B **76**, 079901(E) (2007).

[33] A. Arrott and J. E. Noakes, Phys. Rev. Lett. **19**, 786 (1967).

[34] R. R. Joseph, K. A. Gschneider, Jr., and D. C. Koskimaki, Phys. Rev. B **6**, 3286 (1972).

[35] A. C. Larson and R. B. Van Dreele, Los Alamos National Laboratory Report No. LAUR086-748, 1990 (unpublished).

[36] S. Ohta, T. Kitai, and T. Kaneko, J. Phys.: Condens. Matter **7**, 6809 (1995).

[37] A. Yanase, J. Phys. f: Met. Phys. **16**, 1501 (1986).

[38] M. Higuchi and A. Hasegawa, J. Phys. Soc. Jpn, **65**, 1302 (1996).

[39] S. Blügel, H. Akai, R. Zeller, and P. H. Dederichs, Phys. Rev. B **35**, 3271 (1987).

[40] P. Novák, *"New Notes about Hyperfine Calculations"*, www.wien2k.at/reg-user/textbooks.

[41] D. J. Singh, J. Appl. Phys. **79**, 4818 (1996).

[42] I. I. Mazin and D. J. Singh, Phys. Rev. B **56**, 2556 (1997).

[43] J. Mullally, Struct. Bond. **66**, 1 (1987): *CRC Handbook of Chemistry and Physics*, ed. D. R. Lide, (Taylor and Francis, London, 2005), **9**-77.

[44] B. Coqblin, *"The Electronic Structure of Rare-Earth Metals and Alloys: the Magnetic Heavy Rare-Earths"*, (Academic Press, London, New York, San Francisco, 1977).

[45] G. Cort, R. D. Taylor, and J. O. Willis, J. Appl. Phys. **53**, 2064 (1982).

[46] G. Steinle-Neumann, L. Stixrude and R. E. Cohen, PNAS **101**, 33 (2004).